Design and Optimization of Molecular Nanovalves Based on Redox-Switchable Bistable Rotaxanes

ARTICLE *in* JOURNAL OF THE AMERICAN CHEMICAL SOCIETY · FEBRUARY 2007

Impact Factor: 12.11 · DOI: 10.1021/ja065485r · Source: PubMed

6 AUTHORS, INCLUDING:

yi Liu
Dalian University of Technology
454 PUBLICATIONS **9,101** CITATIONS
SEE PROFILE

Sourav Saha
Florida State University
32 PUBLICATIONS **1,910** CITATIONS
SEE PROFILE

Ken Cham-Fai Leung
Hong Kong Baptist University
84 PUBLICATIONS **3,055** CITATIONS
SEE PROFILE

Jeffrey I Zink
University of California, Los Angeles
470 PUBLICATIONS **21,843** CITATIONS
SEE PROFILE

J|A|C|S
ARTICLES
Published on Web 01/03/2007

Design and Optimization of Molecular Nanovalves Based on Redox-Switchable Bistable Rotaxanes

Thoi D. Nguyen, Yi Liu, Sourav Saha, Ken C.-F. Leung, J. Fraser Stoddart,* and Jeffrey I. Zink*

Contribution from the California NanoSystems Institute and Department of Chemistry and Biochemistry, University of California, Los Angeles, 405 Hilgard Avenue, Los Angeles, California 90095-1569

Received July 29, 2006; E-mail: zink@chem.ucla.edu

Abstract: Redox-controllable molecular nanovalves based on mesoporous silica nanoparticles have been fabricated, using two bistable [2]rotaxanes with different spacer lengths between their recognition sites as the gatekeepers. Three different linkers with varying chain lengths have been employed to attach the bistable [2]rotaxane molecules covalently to the silica substrate. These nanovalves can be classified as having IN or OUT locations, based on the positions of the tethered bistable [2]rotaxanes with respect to the entrances to the nanopores. The nanovalves are more efficient when the bistable [2]rotaxane-based gatekeepers are anchored deep within (IN) the pores than when they are attached closer to (OUT) the pores' orifices. The silica nanopores can be closed and opened by moving the mechanically interlocked ring component of the bistable [2]rotaxane closer to and away from the pores' orifices, respectively, a process which allows luminescent probe molecules, such as coumarins, tris(2-phenylpyridine)iridium, and rhodamine B, to be loaded into or released from the mesoporous silica substrate on demand. The lengths of the linkers between the surface and the rotaxane molecules also play a critical role in determining the effectiveness of the nanovalves. The shorter the linkers, the less leaky are the nanovalves. However, the distance between the recognition units on the rod section of the rotaxane molecules does not have any significant influence on the nanovalves' leakiness. The controlled release of the probe molecules was investigated by measuring their luminescence intensities in response to ascorbic acid, which induces the ring's movement away from the pores' orifices, and consequently opens the nanovalves.

Introduction

A valve is a machine constructed by combining a movable element that regulates the flow of gases or liquids with a reservoir which can also serve as a supporting platform for the movable element. The effectiveness of the valve in controlling the flow is highly dependent on the fitting and matching of these components; if too loose, the valve leaks, and if too tight, it will not open. Construction of such a device on the nanoscale[1−3] requires the integration of stable and inert nanocontainers with appropriate moving parts that can act as gatekeepers to regulate molecular transport in to and out of the containers. Strategies for the assembly of nanovalves in which nanoscale movable elements are attached to mesoporous silicate reservoirs have been demonstrated. These movable elements have been shown, for example, to function as a result of the cis/trans isomerization of azobenzene,[4] intermolecular dimerization of coumarins,[5] tethering and untethering of cadmium sulfide nanoparticles,[6] and the expanding and collapsing of heat-responsive polymers.[7] Other systems involve the electrochemical corrosion of a gold membrane in micro-electromechanical systems[8] and the appending of an addressable photosensitive compound to naturally occurring channel proteins.[9] Generally, the mechanical properties of these nanovalves have not been optimized for the release of a variety of probe molecules.

In our own work, we have demonstrated that the integration of mesoporous silica with interpenetrating supermolecules (pseudorotaxanes) or interlocked molecules (bistable rotaxanes) with movable and switchable properties[10−12] produces operating nanovalves. Redox-switchable [2]pseudorotaxanes and bistable [2]rotaxanes, having a cyclobis(paraquat-*p*-phenylene) (CBPQT^{4+}) tetracationic ring, can be tethered to porous silica thin films[13] and to MCM-41[14] to act together as supramolecular and molecular nanovalves, respectively. In addition, we have reported[15] a supramolecular nanovalve system (switchable pseudorotaxane) based on dibenzo[24]crown-8/dialkylammonium ion complexation that responds to a range of bases. Underscoring of the importance of structure/property relationships, the dimensions of the bases play a vital role in the outcome of the operation of these nanovalves, resulting in a supramolecular system that can release luminescent probe molecules at different rates.

In this paper, we (i) report a comparative study of the molecular nanovalves, synthesized from bistable [2]rotaxanes and attached at different positions on the nanostructrued silica, and (ii) expand the structure−property relationships of this class of molecular nanovalves. The effects of constructing nanovalves using silane linkers with different lengths positioned in different regions relative to the silicate pores' orifices on the effective

10.1021/ja065485r CCC: $37.00

release of large and small probe molecules are discussed. The design, the intricate details of construction of these molecular nanovalves, and their corresponding behavior in controlling the entrapment and release of the molecular contents of nanopores serve as a measurement of optimization in regard to this unique class of mechanically operated devices.

Results and Discussion

Nomenclature and Classification. Three different linkers were employed (Figure 1) in this investigation—namely, isocyanatopropyltriethoxysilane (**a**), allyltriethoxysilane (**b**), and chloromethyltriethoxysilane (**c**). Two methods of removing the surfactant from the silica pores—i.e., calcination (C) and solvent extraction (SE)—were used. Two different locations of the linker relative to the pores' orifices are defined: OUT refers to linkers that are located outside the pores and IN refers to the material in which the linkers are attached to the interiors of the pores. For the OUT location, surfactant removal was achieved by solvent extraction after the linkers reacted with the silica. Three different synthetic variations were used to synthesize the IN location. In the first method designated as IN_{CD}, the material was calcined, followed by derivatization (D) with the linker. In the second method designated as IN_{SED}, the surfactant was solvent-extracted, followed by derivatization with the linker. In the third method designated IN_{CoSE}, the linker was incorporated into the material framework during the one-step co-condensation method (Co) followed by solvent extraction. The amount of probe molecules loaded into the pores was measured by weighing the silica particles before and after loading. For rhodamine B probe molecules, the weight of the silica increased by a maximum of about 4−6%. A 4% increase in weight corresponds to 0.08 mmol of rhodamine B in 1 g of silica or about 40 molecules of the probe per pore.

Materials Characterization. Powder XRD confirmed that the MCM-41 materials retain their long-range order after modification with linkers in the two different locations, as shown in the Supporting Information. The materials have a *d*-spacing of 3.4 nm (for the IN_{CoSE} location) and 3.3 nm (for the OUT location) after solvent extraction. The XRD patterns have one strong Bragg peak at $2\theta = 2.7°$ (indexed as {100}), closely matching that reported in the literature and assigned as a 2-D hexagonal mesostructure.[16] The patterns of the material shift slightly to higher angles upon calcination, indicating that a small

(1) For examples of artificial molecular machines, see: (a) *Molecular Motors*; Schliwa, M., Ed.; Wiley-VCH: Weinheim, 2003. (b) Koumura, N.; Zijlstra, R. W. I.; van Delden, R. A.; Harada, N.; Feringa, B. L. *Nature* **1999**, *401*, 152−155. (c) Feringa, B. L.; van Delden, R. A.; Koumura, N.; Geertsema, E. M. *Chem. Rev.* **2000**, *100*, 1789−1816. (d) Koumura, N.; Geertsema, E. M.; van Gelder, M. B.; Meetsma, A.; Feringa, B. L. *J. Am. Chem. Soc.* **2002**, *124*, 5037−5051. (e) van Delden, R. A.; Hurenkamp, J. H.; Feringa, B. L. *Chem. Eur. J.* **2003**, *9*, 2845−2853. (f) ter Wiel, M. K. J.; van Delden, R. A.; Meetsma, A.; Feringa, B. L. *J. Am. Chem. Soc.* **2003**, *125*, 15076−15086. (g) de Jong, J. J. D.; Lucas, L. N.; Kellogg, R. M.; van Esch, J. H.; Feringa, B. L. *Science* **2004**, *304*, 278−281. (h) Fletcher, S. P.; Dumur, F.; Pollard, M. M.; Feringa, B. L. *Science* **2005**, *310*, 80−82. (i) van Delden, R. A.; ter Wiel, M. K. J.; Pollard, M. M.; Vicario, J.; Koumara, N.; Feringa, B. L. *Nature* **2005**, *437*, 1337−1339. (j) Vicario, J.; Katsonis, N.; Ramon, B. S.; Bastiaansen, C. W. M.; Broer, D. J.; Feringa, B. L. *Nature* **2006**, *440*, 163. (k) Browne, W. R.; Feringa, B. L. *Nat. Nanotechnol.* **2006**, *1*, 26−35. (l) Bermudez, V.; Capron, N.; Gase, T.; Gatti, F. G.; Kajzar, F.; Leigh, D. A.; Zerbetto, F.; Zhang, S. *Nature* **2000**, *406*, 608−611. (m) Brower, A. M.; Frochot, C.; Gatti, F. G.; Leigh, D. A.; Mottier, L.; Paolucci, F.; Roffia, S.; Wurpel, G. W. H. *Science* **2001**, *291*, 2124−2128. (n) Leigh, D. A.; Wong, J. K. Y.; Dehez, F.; Zerbetto, F. *Nature* **2003**, *424*, 174−179. (o) Gatti, F. G.; Len, S.; Wong, J. K. Y.; Bottari, G.; Altieri, A.; Morales, M. A. F.; Teat, S. J.; Frochot, C.; Leigh, D. A.; Brower, A. M.; Zerbetto, F. *Proc. Natl. Acad. Sci. U.S.A.* **2003**, *100*, 10−14. (p) Pérez, E. M.; Dryden, D. T. F.; Leigh, D. A.; Teobaldi, G.; Zerbetto, F. *J. Am. Chem. Soc.* **2004**, *126*, 12210−12211. (q) Berná, J.; Leigh, D. A.; Lubomska, M.; Mendoza, S. M.; Pérez, E. M.; Rudolf, P.; Teobaldi, G.; Zerbetto, F. *Nat. Mater.* **2005**, 704−710. (r) Godinez, C. E.; Zepeda, G.; Garcia-Garibay, M. A. *J. Am. Chem. Soc.* **2002**, *124*, 4701−4707. (s) Dominguez, Z.; Dang, H.; Strouse, M. J.; Garcia-Garibay, M. A. *J. Am. Chem. Soc.* **2002**, *124*, 7719−7727. (t) Balzani, V.; Credi, A.; Raymo, F. M.; Stoddart, J. F. *Angew. Chem., Int. Ed.* **2000**, *39*, 3348−3391. (u) Tseng, H.-R.; Stoddart J. F. In *Modern Arene Chemistry*; Astruc, D., Ed.; Wiley-VCH: Weinheim, 2002; pp 574−599. (v) Flood, A. H.; Ramirez, R. J. A.; Deng, W.-Q.; Muller, R. P.; Goddard, W. A., III; Stoddart, J. F. *Aust. J. Chem.* **2004**, *57*, 301−322. (w) Moonen, N. W. P.; Flood, A. H.; Fernandez, J. M.; Stoddart, J. F. *Top. Curr. Chem.* **2005**, *262*, 99−132. (x) Braunschweig, A. B.; Northrop, B. H.; Stoddart, J. F. *J. Mater. Chem.* **2006**, *16*, 32−44. (y) Saha, S.; Stoddart, J. F. In *Functional Organic Materials—Synthesis, Strategies, and Applications*; Bunz, U. H. F., Müller, T. J. J., Eds.; Wiley-VCH: Weinheim, 2007; pp 295−327. (z) Hawthorne, M. F.; Zink, J. I.; Skelton, J. M.; Bayer, M. J.; Liu, C.; Livshits, E.; Baer, R.; Neuhauser, D. *Science* **2004**, *303*, 1849−1852.

(2) For examples of mesoporous materials, see: (a) Dave, B. C.; Soyez, H.; Miller, J. M.; Dunn, B.; Valentine, J. S.; Zink, J. I. *Chem. Mater.* **1995**, *7*, 1431−1434. (b) Yaghi, O. M.; O'Keeffe, M.; Ockwig, N. W.; Chae, H. K.; Eddaoudi, M.; Kim, J. *Nature* **2003**, *423*, 705−714. (c) Li, H.; Kim, J.; Yaghi, O. M. *Angew. Chem., Int. Ed.* **2003**, *42*, 1819−1821. (d) Duren, T.; Sarkisov, L.; Yaghi, O. M.; Snurr, R. Q.; *Langmuir* **2004**, *20*, 2683−2689. (e) Rowsell, J.; Yaghi, O. M. *Angew. Chem., Int. Ed.* **2005**, *44*, 4670−4679. (f) Rowsell, J.; Spenser, E.; Eckert, J.; Howard, J. A. K.; Yaghi, O. M. *Science* **2005**, *309*, 1350−1354. (g) Cote, A. P.; Benin, A.; Ockwig, N.; Matzger, A.; O'Keeffe, M.; Yaghi, O. M. *Science* **2005**, *310*, 1166−1170. (h) Chen, B.; Liang, C.; Yang, J.; Yaghi, O. M. *Angew. Chem., Int. Ed.* **2006**, *118*, 1390−1393. (i) Sudik, A.; Cote, A.; Wong-Foy, A.; O'Keeffe, M.; Yaghi, O. M. *Angew. Chem., Int. Ed.* **2006**, *118*, 2590−2595.

(3) (a) Joachim, C.; Gimzewski, J. K.; Aviram, A. *Nature* **2000**, *408*, 541−548. (b) Joachim, C.; Gimzewski, J. K. *Struct. Bonding* **2002**, *99*, 1−18. (c) Loppacher, C.; Bammerlin, M.; Gussisberg, M.; Meyer, E.; Güntherodt, H. J.; Lüthi, R.; Schlittler, R.; Gimzewski, J. K.; Tang, H.; Joachim, C. *Phys. Rev. Lett.* **2003**, *90*, 66107−66114. (d) Azov, V. A.; et al. *Adv. Funct. Mater.* **2006**, *16*, 147−156.

(4) Liu, N.; Dunphy, D. R.; Atanassov, P.; Bunge, S. D.; Chen, Z.; López, G. P.; Boyle, T. J.; Brinker, C. J. *Nano Lett.* **2004**, *4*, 551−554.

(5) Mal, N. K.; Fujiwara, M.; Tanaka, Y. *Nature* **2003**, *421*, 350−353.

(6) Lai, C.-Y.; Trewyn, B. G.; Jeftinija, D. M.; Jeftinija, K.; Xu, S.; Jeftinija, S.; Lin, V. S.-Y. *J. Am. Chem. Soc.* **2003**, *125*, 4451−4459.

(7) Fu, Q.; Rama Rao, G. V.; Ista, L. K.; Wu, Y.; Andrzejewski, B. P.; Sklar, L. A.; Ward, T. L.; López, G. P. *Adv. Mater.* **2003**, *15*, 1262−1266.

(8) Santini, J. T., Jr.; Cima, M. J.; Langer, R. *Nature* **1999**, *397*, 335−338.

(9) Kocer, A.; Walko, M.; Meijberg, W.; Feringa, B. L. *Science* **2005**, *309*, 755−758.

(10) (a) Collier, C. P.; Wong, E. W.; Belohradsky, M.; Raymo, F. M.; Stoddart, J. F.; Kuekes, P. J.; Williams, R. S.; Heath, J. R. *Science* **1999**, *285*, 391−394. (b) Collier, C. P.; Mattersteig, G.; Wong, E. W.; Luo, Y.; Beverly, K.; Sampaio, J.; Raymo, F. M.; Stoddart, J. F.; Heath, J. R. *Science* **2000**, *289*, 1172−1175. (c) Pease, A. R.; Jeppesen, J. O.; Stoddart, J. F.; Luo, Y.; Collier, C. P.; Heath, J. R. *Acc. Chem. Res.* **2001**, *34*, 433−444. (d) Tseng, H.-R.; Wu, D.; Fang, N. X.; Zhang, X.; Stoddart, J. F. *ChemPhysChem* **2004**, *5*, 111−116. (e) Flood, A. H.; Stoddart, J. F.; Steuerman, D. W.; Heath, J. R. *Science* **2004**, *306*, 2055−2056. (f) Mendez, P. M.; Flood, A. H.; Stoddart, J. F. *Appl. Phys. A* **2005**, *80*, 1197−1209. (g) Choi, J. W.; Flood, A. H.; Steuerman, D. W.; Nygaard, S.; Braunschweig, A. B.; Moonen, N. N. P.; Laursen, B. W.; Luo, Y.; DeIonno, E.; Peters, A. J.; Jeppesen, J. O.; Xe, K.; Stoddart, J. F.; Heath, J. R. *Chem. Eur. J.* **2006**, *12*, 261−279. (h) Flood, A. H.; Wong, E. W.; Stoddart, J. F. *Chem. Phys.* **2006**, *324*, 280−290. (i) DeIonno, E.; Tseng, H.-R.; Harvey, D. D.; Stoddart, J. F.; Heath, J. R. *J. Phys. Chem. B* **2006**, *110*, 7609−7612.

(11) (a) Bissell, R. A.; Córdova, E.; Kaifer, A. E.; Stoddart, J. F. *Nature* **1994**, *369*, 133−137. (b) Martínez-Díaz, M.-V.; Spencer, N.; Stoddart, J. F. *Angew. Chem., Int. Ed. Engl.* **1997**, *36*, 1904−1907. (c) Ashton, P. R.; Ballardini, R.; Balzani, V.; Credi, A.; Dress, R.; Ishow, E.; Kocian, O.; Preece, J. A.; Spencer, N.; Stoddart, J. F.; Venturi, M.; Wenger, S. *Chem. Eur. J.* **2000**, *6*, 3558−3574. (d) Balzani, V.; Clemente-León, M.; Credi, A.; Ferrer, B.; Venturi, M.; Flood, A. H.; Stoddart, J. F. *Proc. Natl. Acad. Sci. U.S.A.* **2006**, *103*, 1178−1183. (e) Balzani, V.; Clemente-León, M.; Credi, A.; Semeraro, M.; Venturi, M.; Tseng, H.-R.; Wenger, S.; Saha, S.; Stoddart, J. F. *Aust. J. Chem.* **2006**, *59*, 193−206.

(12) (a) Chia, S.; Cao, J.; Stoddart, J. F.; Zink, J. I. *Angew. Chem., Int. Ed.* **2001**, *40*, 2447−2451. (b) Saha, S.; Johansson, L. E.; Flood, A. H.; Tseng, H.-R.; Zink, J. I.; Stoddart, J. F. *Small* **2005**, *1*, 87−90. (c) Saha, S.; Johansson, E.; Flood, A. H.; Tseng, H.-R.; Zink, J. I.; Stoddart, J. F. *Chem. Eur. J.* **2005**, *11*, 6846−6858.

(13) Hernandez, R.; Tseng, H.-R.; Wong, J. W.; Stoddart, J. F.; Zink, J. I. *J. Am. Chem. Soc.* **2004**, *126*, 3370−3371.

(14) Nguyen, T. D.; Tseng, H.-R.; Celestre, P. C.; Flood, A. H.; Liu, Y.; Stoddart, J. F.; Zink, J. I. *Proc. Natl. Acad. Sci. U.S.A.* **2005**, *102*, 10029−10034.

(15) (a) Nguyen, T. D.; Leung, K. C.-F.; Liong, M.; Pentecost, C. D.; Stoddart, J. F.; Zink, J. I. *Org. Lett.* **2006**, *8*, 3363−3366. (b) Leung, K. C.-F.; Nguyen, T. D.; Stoddart, J. F.; Zink, J. I. *Chem. Mater.* **2006**, *18*, 5919−5928.

(16) Van Tendeloo, G.; Lebedev, O. I.; Collart, O.; Cool, P.; Vansant, E. F. *J. Phys.: Condens. Matter* **2003**, *15*, S3037−S3046.

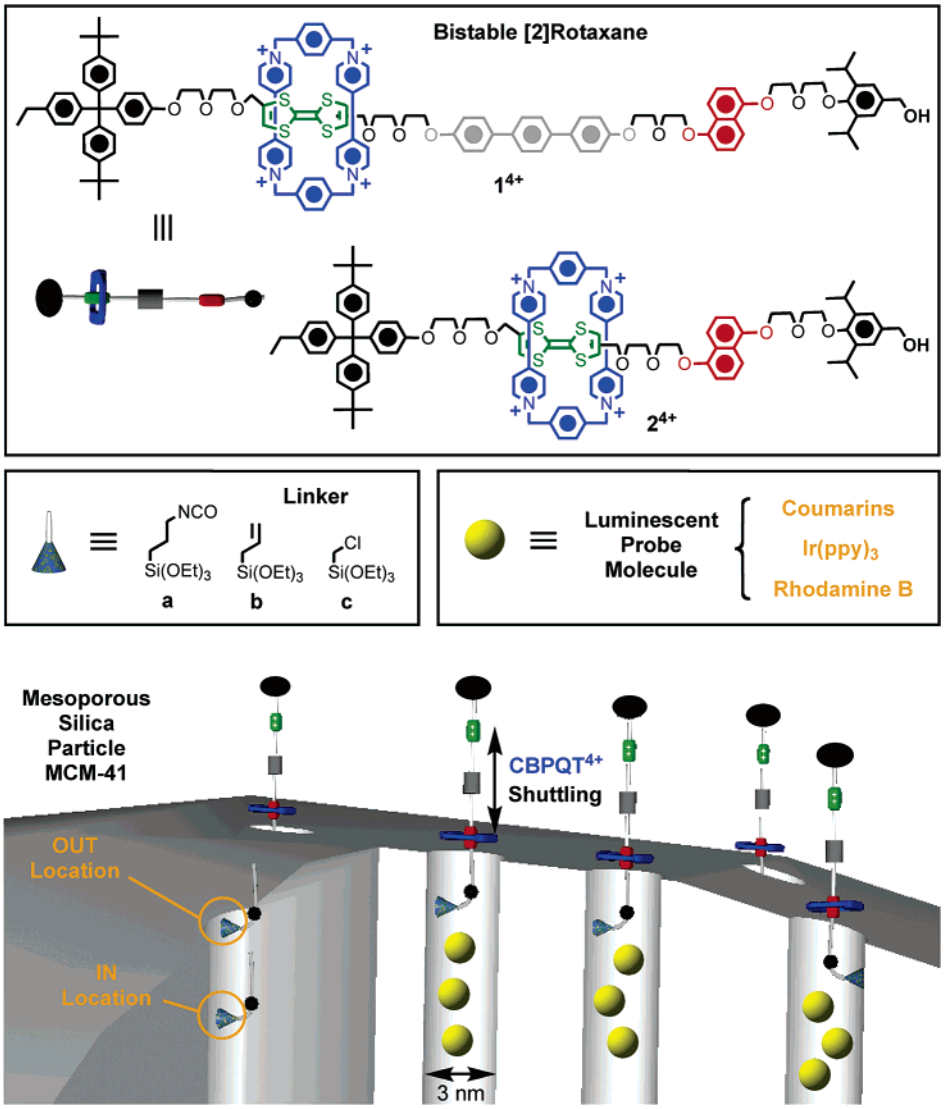

Figure 1. Depiction of the assembly of the components to form nanovalves with the structural formulas of the bistable [2]rotaxanes $\mathbf{1}^{4+}$ and $\mathbf{2}^{4+}$, the three silane linkers **a**, **b**, and **c** used in this study as well as the graphical representations of luminescent probe molecules and the possible positions (IN and OUT) of the linker relative to the pore orifice. The pores are loaded when the valves are open and the probe molecules are trapped inside the pores when the valves are closed. The trapped molecules are released when the valves are reopened. The cycle can be repeated over and over again.

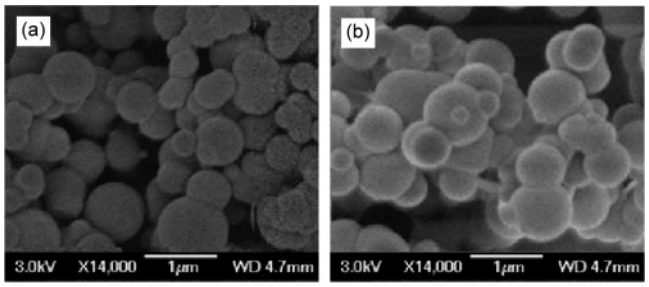

Figure 2. SEM analysis of the MCM-41 porous silica particles with (a) having linkers in the OUT and (b) having linkers in the IN locations.

degree of structure shrinkage occurs. In contrast, solvent extraction does not result in noticeable shifts in the Bragg peaks.[17]

Scanning electron microscopy (SEM) was used (Figure 2) to assess the particle size and particle morphology. SEM shows that the particles are approximately spherical and have diameters ranging from 400 to 900 nm with an average of 550 nm. Reflectance IR spectra were used[18] to monitor derivatization.

Fluorescence spectra of the 1,5-dioxynaphthalene (DNP) unit confirm that the bistable [2]rotaxane $\mathbf{1}^{4+}$ is attached to the surface of an extensively-washed material. The silica-tethered bistable [2]rotaxane $\mathbf{1}^{4+}$ has the same spectroscopic signature as that of $\mathbf{1}^{4+}$ in solution.

N_2 isotherms (at 77 K) were employed to characterize the surface area and the average pore diameter.[19] N_2 isotherms were taken after the samples had undergone solvent extraction and allyltriethoxysilane functionalization. After derivatization with the bistable [2]rotaxane $\mathbf{1}^{4+}$, the isotherms were recorded again. For the material with linkers in the OUT location, the isotherm showed a single N_2 condensation, suggesting that the attached linkers do not hinder the N_2 condensation. In contrast, for the material with the linkers in the IN_{CoSE} and IN_{SED}, the isotherms showed the presence of two N_2 condensation curves. The

(17) Asefa, T.; Maclachlan, M. J.; Coombs, N.; Ozin, G. A. *Nature* **1999**, *402*, 867−871.

(18) Burkett, S. L.; Sims, S. D.; Mann, S. *Chem. Commun.* **1996**, 1367−1368.

(19) Kresge, C. T.; Leonowicz, M. E.; Roth, W. J.; Vartuli, J. C.; Beck, J. S. *Nature* **1992**, *359*, 710−712.

presence of a second condensation curve and a shift of the inflection point to higher pressure indicate a new hindrance in the nanopores, fitting (see Supporting Information) the description that the linkers are tethered to the interior of the nanopores. In all of the experiments, the particles are washed before the release profiles are measured. The washing removes most of the surface-adsorbed guest molecules; in addition, some leakage may occur during that time. The washed material is placed in the cuvette and the luminescence of the solution is monitored for a minimum of 5 min to a maximum of 1 h, before triggering the opening of the nanovalve. Minimal leakage of the nanovalve is defined by a flat baseline over these time periods. The surface silanol coverage of silica particles prepared in a manner similar to ours has been reported to be about 2.4 silanols per 1 nm^2. There are about 7.8 Si atoms/nm^2; thus, roughly one-third of all Si atoms are in the form of silanol. Derivatization using excess of ICPES is almost quantitative. Based on these numbers, there are on average approximately 2−3 pseudorotaxanes around the circumference of a 2 nm diameter pore. The surface area, average pore diameter, and *d*-spacing of allyltriethoxysilane-attached MCM-41 at different locations of the pores are listed in Table 1.

Table 1. Properties of Materials with Linker Allyltriethoxysilane (**b**) in Different Locations

	material			
	surfactant-removed MCM-41	OUT	IN_{CoSE}	IN_{SED}
surface area[a] (m^2/g)	930	1023	1251	1112
average pore diameter[a] (nm)	2.0	2.0	2.3	2.1
d-spacing[b] (nm)	2.9	3.1	3.4	3.1

[a] Obtained from N_2 isotherm. [b] Obtained from powder XRD.

Operation of the Nanovalves. The efficient operation of the molecular nanovalves is strongly dependent on the interplay between the movable element, the supporting silica framework also acting as a reservoir, and the assembly of the molecular components close to the entrances of the nanopores. Cyclobis(paraquat-*p*-phenylene) ($CBPQT^{4+}$), the tetracationic ring which shuttles between the tetrathiafulvalene (TTF) and 1,5-dioxynaphthalene (DNP) units on dumbbell components—or threading and dethreading of the DNP unit in a pseudorotaxane[13]—results in open and closed positions of the molecular- and supramolecular-nanovalves, respectively.[13,14] The molecular nanovalves constitute a collective mechanical system. The fitting and matching of the components is essential for the proper functioning of this collective mechanical system; otherwise, the nanovalves will leak. In this system, the efficient functioning of the nanovalves is highly dependent (Figure 1) on the distance between the movable ring component (i.e., $CBPQT^{4+}$) on the bistable [2]rotaxane molecules and the nanopores' orifices. Controlling this distance by rational molecular design requires the use of an assortment of linkers having different lengths, or the deliberate positioning of the bistable molecules in the nanopores—as a result of the directed placement of the silane linker at a desired position relative to the nanopores' orifices—or a synergistic effect of both. The controlled release behavior of probe molecules from nanovalves designed with different locations has been investigated to gain insight into the optimum design of the molecular nanovalve system.

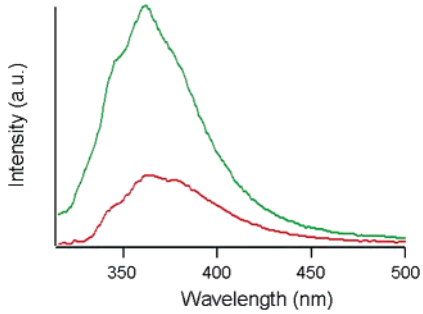

Figure 3. DNP luminescence of the nanovalves in the closed state (bottom) and in the open state (top).

1. Monitoring the Nanovalves' Operation. The operation of the nanovalves can be monitored directly by following the luminescence of the DNP unit. When the nanovalves are closed—that is when the $CBPQT^{4+}$ ring encircles the DNP unit—the luminescence of these DNP units is quenched. The reduction of TTF^{2+} to neutral TTF by ascorbic acid causes the $CBPQT^{4+}$ ring to shuttle to the TTF unit and the DNP-based luminescence intensity increases 3-fold. These spectroscopic results show (Figure 3) that the $CBPQT^{4+}$ rings move and the nanovalves function in all of the IN and OUT locations.

2. Effect of the Sizes of Probe Molecules on the Nanovalves' Operation. The tightness of the closed nanovalves and their effectiveness in releasing molecules, when opened, were examined using probe molecules of different sizes. In a previous communication[14] dealing with molecular nanovalves based on an IN_{CD} location using the isocyanatopropyltriethoxysilane (ICPES) linker, the time-dependent releases (release profiles) of the luminescent probe molecules, rhodamine B (a cationic compound, Figure 4a) and $Ir(ppy)_3$ (a neutral coordination compound, Figure 4b), were characterized by a flat baseline

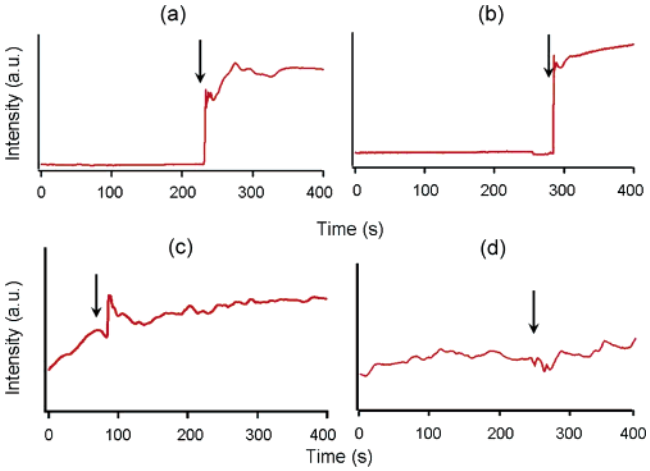

Figure 4. Release profiles of the nanovalves **1a**-IN_{CD} during the release of (a) rhodamine B, (b) $Ir(ppy)_3$, (c) coumarin 460, and (d) coumarin 440 with time. The arrow indicates the time for the addition of a reducing agent (ascorbic acid) to trigger the release. All materials were washed extensively previously. On account of the leaky nature of nanovalves (c) and (d), most coumarins had already leaked out.

prior to activation, followed by rapid release of the probe molecules on reduction with ascorbic acid. The observation of a flat baseline, in advance of opening the nanovalves, indicates that they are tightly closed and so prevent the probe molecules from leaking out. The response times for the triggered releases of rhodamine B and $Ir(ppy)_3$ were similar, indicating that the

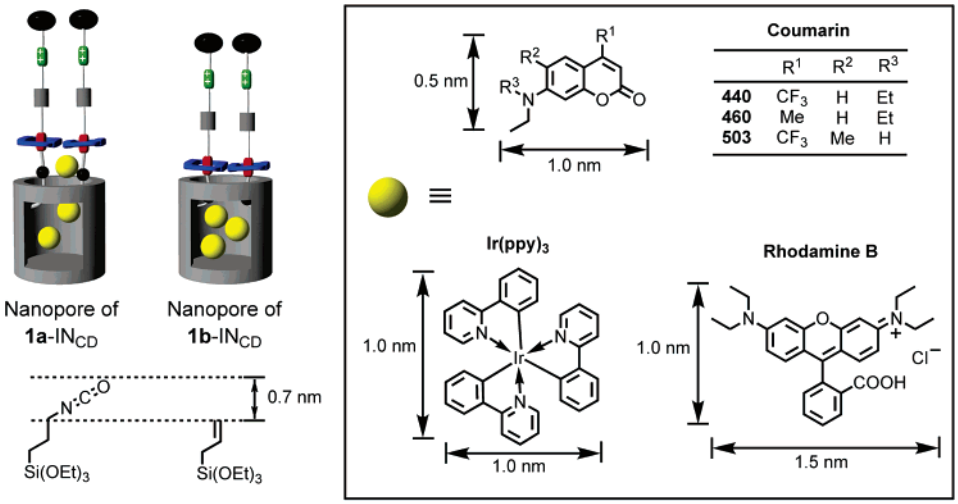

Figure 5. Graphical representation of the nanopores of **1a**-IN$_{CD}$ and **1b**-IN$_{CD}$ with fluorescent probe molecules trapped inside the nanopores. The luminescent guests come in different sizes: the coumarins are small molecules, while Ir(ppy)$_3$ and rhodamine B are larger molecules. The allyltriethoxysilane (**b**) linker is 0.7 nm shorter than the isocyanatopropyltriethoxysilane (**a**). Nanovalves constructed from allyltriethoxysilane have the CBPQT^{4+} ring located closer to the orifices than those constructed with the isocyanatopropyltriethoxysilane linker.

releases are not sensitive to the charges on the probe molecules. Both rhodamine B and Ir(ppy)$_3$ have similar molecular dimensions. The CBPQT^{4+} rings were close enough to the pores' orifices, relative to the size of the trapped probe molecules, to create tightly fitting molecular nanovalves.

Coumarins, a group of neutral fluorophores with molecular dimensions significantly smaller than those of rhodamine B and Ir(ppy)$_3$, and stable under the nanovalves' operating conditions,[20] were selected for further testing of the nanovalves. Two different coumarins—coumarins 440 and 460—with slight differences in their molecular structures were selected. The preparation of the nanovalves, the loading of the probes, and the operation of the nanovalves were the same as those used in the experiments using rhodamine B and Ir(ppy)$_3$.

The controlled release profiles of both coumarin guests show that the nanovalves leak, as evidenced by the rise in the luminescence intensities of the coumarins compared with the situation before the nanovalves are opened (Figure 4c). The addition of ascorbic acid at 100 s to open the nanovalves results in little or no additional increase in the coumarins' luminescence intensities. In all cases, shuttling of the CBPQT^{4+} ring from the DNP to the TTF unit was observed, as monitored by the increase in the DNP luminescence intensity. The nanovalves in the IN$_{CD}$ location trap the larger rhodamine B and Ir(ppy)$_3$ guest molecules effectively but do not trap the smaller coumarins.

A simple analysis of the relative sizes of the nanovalves' components is revealing. For a pore with an average diameter of about 2 nm, a ring with a cross dimension of about 1 nm such as the CBPQT^{4+} ring is able to block the opening.[21] Rhodamine B has long and short dimensions of 1.5 and 1 nm, respectively, and Ir(ppy)$_3$ is roughly spherical with a diameter of 1 nm. However, the coumarin probes have significantly smaller sizes[21] of about 1.0 × 0.5 nm. Because of these size differences between the probe molecules, the larger probe molecules are trapped by the closed nanovalves, but the smaller ones leak out. These observations suggest that when the nanovalves are closed, the CBPQT^{4+} ring is too far from the nanopores' orifices to trap the small coumarin guests. Shortening the length of the linker (Figure 5) is a design option to reduce leaks of this nature.

3. Controlling Leaks by Shortening Linker Lengths. Redesigning of the nanovalves for trapping small probe molecules necessitates the positioning of the ring closer to the nanopores' orifices. This change can be achieved by using linkers that are shorter and less flexible than that emanating from isocyanatopropyltriethoxysilane (**a**). Among many triethoxysilyl linkers, those produced from allyltriethoxysilane (**b**) and chloromethyltriethoxysilane (**c**) were chosen since they are significantly shorter than those emanating from isocyanatopropyltriethoxysilane (**a**)—by 0.7 nm—and should provide the necessary shorter distance from the ring to the pores' orifices and a higher degree of rigidity to prevent the coumarin guests from leaking. Both allyl and chloromethyl functional groups react with the arylmethylhydroxyl end of the [2]rotaxane **1**$^{4+}$ to yield ether linkages through acid-catalyzed or base-assisted reactions.[22,23]

Nanovalves were synthesized using the shorter chain reagents **b** and **c**. The triggered release of coumarin 460 from **1a**-IN$_{CD}$ and **1b**-IN$_{CD}$ nanovalves was monitored by recording the emission spectra—Figures 6a and 6b, respectively—of the solution above the hybrid material. In the case of **1b**-IN$_{CD}$, no leakage occurred before the nanovalves were opened, as indicated (Figure 6b) by a flat baseline. When the nanovalves were activated by the addition of 30 μL of ascorbic acid solution, the emission intensities increased rapidly, showing that the guest molecules were released from the nanopores and escaped into the solution. However, **1a**-IN$_{CD}$ nanovalves were shown to be the leaky ones, as revealed from the increasing baseline intensity (Figure 6a), even before being activated by ascorbic acid.

Similar results were obtained when chloromethyltriethoxysilane (**c**) was used to construct the nanovalves. The large

(20) The tested coumarin was dissolved in MeCN and treated with both ascorbic acid and Fe(ClO$_4$)$_3$. The luminescence spectra of coumarin before and after the addition of these agents were then compared with each other. There were no changes in the coumarin's luminescence intensities nor shifting of the luminescence peaks.
(21) As determined using Chem3D Ultra (MM2 Calculation).
(22) Kresge, A. J.; Chiang, Y.; Fitzgerald, P. H.; McDonald, R. S.; Schmid, G. H. *J. Am. Chem. Soc.* **1971**, *93*, 4907−4908.
(23) Liepins, E.; Ancens, G.; Erchak, N. P.; Lukevics, E. *Zh. Obshch. Khim.* **1988**, *58*, 384−393.

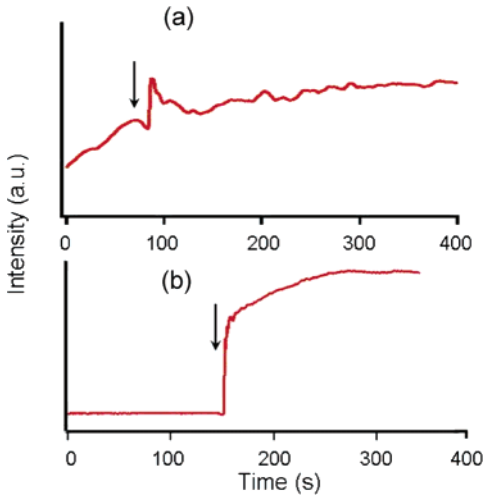

Figure 6. Trapping and release of coumarin 460 by the (a) **1a**-IN_{CD} nanovalves and (b) **1b**-IN_{CD} nanovalves. The arrow indicates the time at which the ascorbic acid activating agent was added to open the valve. Whereas the release profile of the **1a**-IN_{CD} nanovalves is leaky, that of the **1b**-IN_{CD} nanovalves is tight.

rhodamine B molecules were also trapped without leakage and released upon activation of the nanovalves re-designed with the short linkers.

Another variation of the nanovalves **1b**-IN_{CD} using the shorter bistable [2]rotaxane $\mathbf{2}^{4+}$ was investigated to demonstrate the versatility of this class of nanovalves and to confirm the importance of the linker lengths. The short bistable [2]rotaxane $\mathbf{2}^{4+}$ differs from $\mathbf{1}^{4+}$ in the lack of the terphenyl spacer connecting the TTF and DNP stations. This shortening of the rotaxane in **2b**-IN_{CD} should provide the same function and operation as **1b**-IN_{CD} since, in the closed state, the $CBPQT^{4+}$ ring is still positioned at a distance from the nanopores' openings similar to that of **1b**-IN_{CD}. The triggered release profile of the coumarin 460 from nanovalves **2b**-IN_{CD} is similar to that of the nanovalves **1b**-IN_{CD}, indicating that the variation in the length between the TTF and the DNP recognition sites in the dumbbell of the bistable [2]rotaxanes does not affect the functioning of the nanovalves.

4. Controlling Leaks by Positioning the Linkers. The ability of the nanovalves to trap molecules is highly dependent on the distance between the movable component ($CBPQT^{4+}$) and the nanopores' orifices. Shortening the distance between the rings and the nanopores, by using shorter linkers, can control the triggered release of coumarin 460 with no leakage. Another way of controlling the distance between the rings and the nanopores can be achieved by positioning the linker either further inside the nanopores, thus shortening the distance between the rings and the nanovalves, or outside the nanopores, thus extending the distance between the rings and the nanovalves. Methods of organic functionalization of MCM-41 with linkers by either co-condensation or postsynthetic grafting offer the means of achieving these deliberate placements of the linkers.[18,25a] Despite intensive effort, achieving linker coverage exclusively at a specific location remains elusive. Rather, a distribution of linkers' overall positions is observed for both co-condensation and postsynthesis methods. The deliberate placement of the movable element relative to the openings of nanopores and its effect on the leakiness of the nanovalves were investigated. The results of this investigation will now be discussed.

The bistable rotaxane's anchoring position is dictated by the position of the linker. The further into the interior of the nanopores the linker is bonded, the shorter the distance between the movable element ($CBPQT^{4+}$) and the nanopores' orifices. Organic functionalization of MCM-41 by co-condensation with the linker offers a means to achieve this state. Linkers incorporated by co-condensation will align the nanopores' walls of the MCM-41 on account of the propensity of the polar/nonpolar environments of the linker to form micelle-like frameworks.[18,24] After the extraction of surfactant from the MCM-41, the linkers are attached to the nanopores' walls, with the active ends extending into the void space of the nanopores. Although the material synthesized by co-condensation method has linkers that predominantly occupy the nanopores' walls, a minority of the linkers is distributed outside the walls.[25a] Since the nanovalves with bistable [2]rotaxanes tethered to these outside linkers are leaky, their contents are washed away after successive washings. As a result, the release profile of the nanovalves obtained by using co-condensation reflects only the portion of the nanovalves which are capable of trapping probe molecules.

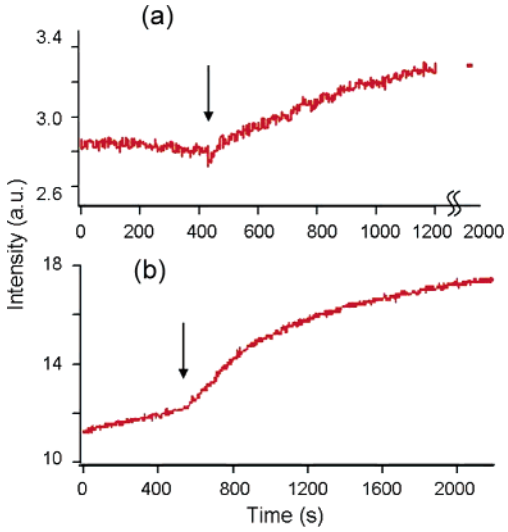

Figure 7. Release profiles of coumarin 460 over time from the nanovalves (a) **1a**-IN_{CoSE} and (b) **1a**-OUT. The arrow indicates the time at which ascorbic acid was added. In (a), after the first 1200 s, another luminescence spectrum with the intensity shown as a point was obtained at 2000 s. Whereas (a) shows no leakage, (b) shows a large amount of leakage, as indicated by the premature rise in luminescence intensities.

The release profile of coumarin 460 from nanovalves **1a**-IN_{CoSE} is shown in Figure 7a. Employing the ICPES linker, deliberate placement of the bistable [2]rotaxanes in the interior of the nanopores produces nanovalves which do not leak. Upon addition of ascorbic acid, the nanovalves release the trapped coumarins into the solution, as indicated by the increase in luminescence intensities. The total time required to release the nanopores' contents is substantially longer than that for the nanovalves **1b**-IN_{CD}, suggesting the slower rate of release of probe molecules located deep inside the nanopores. The smaller

(24) (a) Minoofar, P. N.; Hernandez, R.; Chia, S.; Dunn, B.; Zink, J. I.; Franville, A.-C. *J. Am. Chem. Soc.* **2002**, *124*, 14388−14396. (b) Hernandez, R.; Franville, A.-C.; Minoofar, P.; Dunn, B.; Zink, J. I. *J. Am. Chem. Soc.* **2001**, *123*, 1248−1249.
(25) (a) Lim, M. H.; Stein, A. *Chem. Mater.* **1999**, *11*, 3285−3295. (b) Mal, N. K.; Fujiwara, M.; Tanaka, Y.; Taguchi, T.; Matsukata, M. *Chem. Mater.* **2003**, *15*, 3385−3394.

numbers of probe molecules that were released indicated that the nanopores are substantially occupied by the linkers and so contain a smaller load.

The production of nanovalves **1a**-OUT is favored if the MCM-41 particles are derivatized when the surfactants occupy the inside of the nanopores, i.e., before calcination or solvent extraction. In this case, the linkers will not be able to react with the interior of the nanopores and will be restricted to the outer surfaces of the nanopores and the nanopores' entrances.[25b] In these nanovalves, the linkers were prevented from entering the nanopores and the distance between the nanopores' openings and the $CBPQT^{4+}$ ring were maximized. For MCM-41, the surfactants occupied the inner spaces of the nanopores and blocked access to them.[25b] When the linkers are treated with the MCM-41 at this stage, the linkers react only with the surface silanol outside of the nanopores' interiors. After the derivatization, solvent extraction was used to remove the surfactants. The N_2 isotherm of this kind of material has one N_2 condensation profile, confirming that the nanopores are empty. The material was then functionalized with the bistable [2]rotaxanes.

In contrast with the controlled release of coumarin 460 from the nanovalves **1a**-IN_{CoSE}, for which no leakage was observed (Figure 7a), the nanovalves **1a**-OUT show a substantial amount of leakage of coumarin 460, as indicated (Figure 7b) by the increase of luminescence intensities. Upon activation, a substantial increase in the rate of release is observed. The total increase in intensities, both from the leakage and from the nanopores when the nanovalves are opened, is at least one order of magnitude larger than that observed in the case of the nanovalves **1a**-IN_{CoSE}. This increase in luminescence intensities arises because the nanopores with the bistable [2]rotaxanes at the OUT location can contain more probe molecules than that involving the IN location.

5. Optimized Location of Nanovalves. In this section, the properties of **1b**-MCM-41 nanovalves will be compared to other nanovalves. The controlled release profiles of the **1b**-MCM-41 nanovalves in all three locations are shown in Figure 8. The baselines are all flat, indicating that no leakage of the probe molecules occurs from the nanovalves within 100 s. For the **1b**-OUT nanovalves, the release of coumarin 460 from the nanopores upon activation with ascorbic acid is characterized by a large and fast increase in the luminescence intensities, indicating that a large amount of probe molecules was released, followed by a short tapering off in the intensity in the next few hundreds of seconds. In contrast, the release profiles of coumarin 460 from the **1b**-IN_{SED} and **1b**-IN_{CoSE} nanovalves are observed with a smaller increase in their luminescence intensities. All three samples were measured once again after several hours elapsed to determine the maximum intensities. The total amount of coumarin 460 released from the OUT location is one order of magnitude higher than those from the IN_{SED} and the IN_{CoSE} locations.

The release profiles from three different locations indicate that the positioning of the bistable [2]rotaxane $\mathbf{1}^{4+}$ in the OUT location produces nanovalves which are superior to those in which $\mathbf{1}^{4+}$ is in the IN_{CoSE} and the IN_{SED} locations. The OUT location releases a much larger amount of coumarin 460 than those in the IN_{CoSE} and IN_{SED} locations. The nanopores of the **1b**-OUT nanovalves contain a larger load of coumarin than those in the IN_{CoSE} and IN_{SED} locations, where a substantial amount

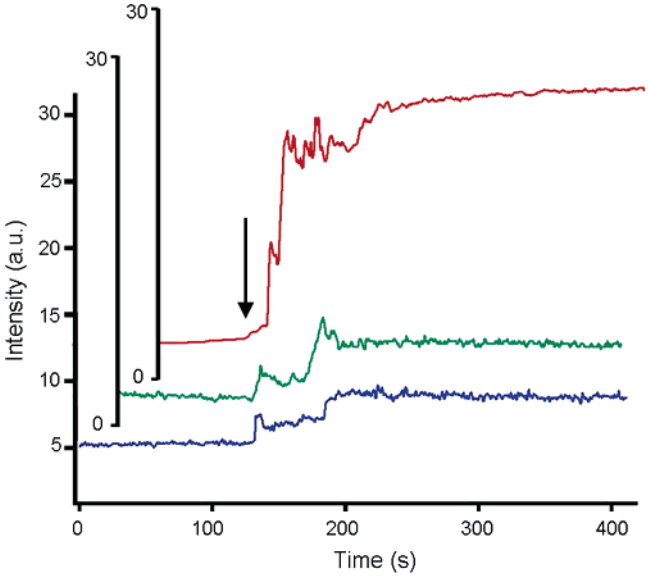

Figure 8. Controlled release of coumarin 460 from the nanovalves **1b**-OUT (top), **1b**-IN_{CoSE} (middle), and **1b**-IN_{SED} (bottom). The arrow indicates the time at which the reducing agent was added to open the nanovalves. Nanovalves in the OUT location release a much larger load of the probe molecules.

of the nanopores' volume is occupied by the linkers. This observation is consistent with the N_2 isotherms, which clearly differentiate between the OUT and IN locations.

The effect of linkers' derivatization on the amount of the load was observed for the nanovalves constructed from both long and short linkers. This similarity indicates that it is the methods behind the linkers' deliberate placements that control the amount of the load, a feature which enhances the applicability of this class of nanovalves.

Concluding Remarks

The ability to fine-tune different parts of nanoscale molecular machines—in this case of molecular nanovalves—has been well-demonstrated by means of rational design and the operation of nanovalves to achieve optimal functions. This rational design extends the concept of tuning in these nanovalves as a result of placing the linkers in specific locations to release large and small guest molecules. It can be expressed as a general trend: small guest molecules require short linkers and large guest molecules require long linkers. The components can also be redesigned further with different aspect ratios to place the movable

Table 2. Relationship between Length of the Linkers, Size of the Guest Molecules, and the Effectiveness of the Nanovalves

attachment	linker[a]	probe	leakage
IN_{CD}	**a**	rhodamine B	no
IN_{CD}	**a**	$Ir(ppy)_3$	no
IN_{CD}	**a**	coumarin 440	yes
IN_{CD}	**a**	coumarin 460	yes
IN_{CD}	**b**	coumarin 460	no
IN_{CD}	**c**	rhodamine B	no
IN_{CD}	**c**	coumarin 460	no
IN_{CoSE}	**a**	coumarin 460	no
OUT	**a**	coumarin 460	yes
OUT[b]	**b**	coumarin 460	no
IN_{CoSE}	**b**	coumarin 460	no
IN_{SED}	**b**	coumarin 460	no

[a] Linker structures are shown in Figure 1. [b] Maximum pore volume.

Scheme 1. Procedures for the Construction and Operation of the Nanovalves **1a/b/c**-IN_{CoSE}[a]

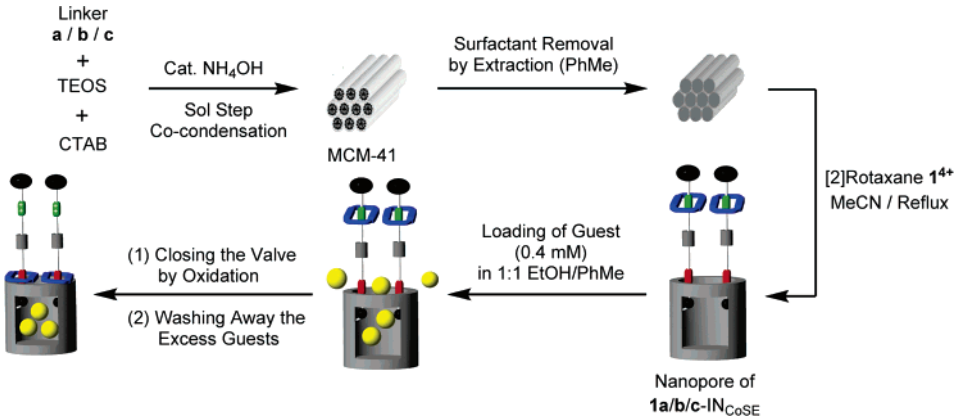

[a] First, TEOS, CTAB, and the linker (**a**, **b**, or **c**) are co-condensed in the presence of a catalytic amount of NH_4OH to afford the silica particles MCM-41. Extraction of the silica particles MCM-41 with PhMe affords the surfactant-removed, mesoporous silica particles. Derivatization of the bistable [2]rotaxanes $\mathbf{1}^{4+}$ with the mesoporous silica particles gives the **1a**/**b**/**c**-IN_{CoSE} nanovalves. The nanovalves **1a**/**b**/**c**-IN_{CoSE} are loaded with guest molecules and closed by oxidation on the TTF unit.

components in different locations relative to the nanopores—namely, the IN_{CoSE}, the IN_{CD}, the IN_{SED}, and the OUT locations. The results are summarized in Table 2. These locations can be differentiated and are expressed strongly in different release profiles. This ability to fine-tune and control the nanovalves' aspect ratios is fundamental and essential to the future design of drug delivery systems that can release drugs with different structural dimensions.

Experimental Section

Materials. The bistable [2]rotaxane[14] $\mathbf{1}^{4+}$ and the much shorter bistable [2]rotaxane[26] $\mathbf{2}^{4+}$ were synthesized according to the literature procedures. Distilled and deionized H_2O were obtained from Millipore. Other analytical and reagent grade chemicals were purchased from the following suppliers: tetraethoxysilane (TEOS, 98%, Aldrich), cetyltrimethylammonium bromide (CTAB, ≥99%, Aldrich), isocyanatopropyltriethoxysilane (**a**) (ICPES, 95%, Aldrich, redistilled prior to use), allyltriethoxysilane (**b**) (Gelest), chloromethyltriethoxysilane (**c**) (Gelest), MeCN (≥99.5%, EMD), PhMe (≥99.5%, EMD), NH_4OH solution (28−30%, EMD), EtOH (200 proof, Pharmaco-AAPER), coumarin 440 (Exciton), coumarin 460 (Exciton), coumarin 503 (Exciton), ascorbic acid (≥99%, Sigma), $Fe(ClO_4)_3{\cdot}6H_2O$ (Alfa Aesar), rhodamine B (Lambda Physik), and $Ir(ppy)_3$ (ppy = 2-phenylpyridine).

Instrumentation. Powder X-ray diffraction (XRD) patterns were collected using a Philips X'Pert Pro with Cu Kα radiation. Scanning electron microscopic (SEM) images were collected using a JEOL SM-71010 (fine powder profile). Au coating of the material for SEM imaging was carried out by a gold sputterer (Hummer 6.2, Anatech LTD, plasma discharge current = 15 mA at 70 mTorr for 2 min). N_2 isotherms were measured using a Micromeritics ASAP 2000 (mesoporous material program). The controlled release of probe molecules into solution was monitored over time using luminescence spectroscopy (Acton SpectraPro 2300i, CCD and coherent Krypton Innova I300C and Argon Innova 90C-5 excitation lasers).

General Preparation of the [2]Rotaxane-Derivatized MCM-41. MCM-41 was prepared according to a literature procedure.[27a] The surfactant was removed by either calcination at 550 °C for 5 h or solvent extraction (2.0 g of the material is heated under reflux in MeOH/HCl solution (220 mL of MeOH and 2.5 mL of concentrated HCl)). Attachment or incorporation of a range of molecular compounds onto silica prepared by the sol−gel method have been investigated previously.[27b−g] The surfactant-removed MCM-41 was derivatized with the linker compounds, isocyanatopropyltriethoxysilane (**a**), allyltriethoxysilane (**b**), or chloromethyltriethoxysilane (**c**) in PhMe for 12 h under N_2 (1 atm) using a gas-phase reaction. The powder was placed on a filter above a refluxing PhMe solution (40 mL), containing 2 mL of ICPES and 600 mg of calcined SiO_2. The linker-derivatized material (**a**/**b**/**c**-MCM-41) was soaked in PhMe for 1 d to remove unreacted, surface-adsorbed linker molecules, followed by filtering and drying under reduced pressure. To attach the bistable [2]rotaxane $\mathbf{1}^{4+}$ to MCM-41, the linker-derivatized MCM-41 was placed in a MeCN solution (10 mL) containing 2 mg of $\mathbf{1}^{4+}$ and 200 mg of SiO_2 and heated under reflux for 12 h under N_2 (1 atm). For the isocyanatopropyltriethoxysilane-linked MCM-41 (**a**-MCM-41), the bistable [2]rotaxane $\mathbf{1}^{4+}$ was attached by means of the formation of a carbamate group. For the allyltriethoxysilane-linked MCM-41 (**b**-MCM-41), a catalytic amount of HCl (0.1 mL of 0.01 M HCl) was used to catalyze the coupling reaction with $\mathbf{1}^{4+}$. For the chloromethyltriethoxysilane-linked MCM-41 (**c**-MCM-41), Et_3N (0.5 mL, 3.6 mmol) was used as the coupling reagent in attaching $\mathbf{1}^{4+}$. The resulting MCM-41s were washed extensively. The presence of $\mathbf{1}^{4+}$ was confirmed by the luminescence of the 1,5-dioxynaphthalene unit present in the dumbbell component of the bistable [2]rotaxane.

Derivatized MCM-41 was loaded with guest (luminescence probe) molecules by soaking the derivatized material in 1:1 EtOH/PhMe solutions containing the guest in concentrations ranging from 0.4 to 0.5 mM. Approximately 2 equiv of $Fe(ClO_4)_3{\cdot}6H_2O$ in MeCN was added to the loaded material to close the nanovalves and the solution was filtered quickly. The loaded and closed material was washed with MeCN to remove any surface-adsorbed guest molecules.

Positioning the Linker with the IN_{CoSE} Location. The synthesis of nanovalves with an IN_{CoSE} location is a combination of two separate MCM-41 syntheses. Based on the method described by Grun et al.,[27a] for which NH_4OH is used to give spherical-shaped particles, and the co-condensation modification by Lim et al.,[28a] mesoporous material was synthesized (Scheme 1) with the linkers in the IN_{CoSE} location with nearly the same pore diameter and same morphology as the material synthesized without co-condensed linkers. CTAB (2.5 g) was dissolved

(26) Steuerman, D. W.; Tseng, H.-R.; Peters, A. J.; Flood, A. H.; Jeppesen, J. O.; Nielsen, K. A.; Stoddart, J. F.; Heath, J. R. *Angew. Chem., Int. Ed.* **2004**, *43*, 6486−6491.
(27) (a) Grun, M.; Laner, I.; Unger, K. K. *Adv. Mater.* **1997**, *9*, 254−257. (b) Miller, J. M.; Dunn, B. S.; Valentine, J. S.; Zink, J. I. *J. Non-Cryst. Solids* **1996**, *202*, 279−289. (c) Dave, B. C.; Miller, J. M.; Dunn, B. S.; Valentine, J. S.; Zink, J. I. *J. Sol-Gel Sci. Technol.* **1997**, *8*, 629−634. (d) Dunn, B. S.; Miller, J. M.; Dave, B. C.; Valentine, J. S.; Zink, J. I. *Acta Mater.* **1998**, *46*, 737−741. (e) Chia, S.; Jun, U.; Tamanoi, F.; Dunn, B. S.; Zink, J. I. *J. Am. Chem. Soc.* **2000**, *122*, 6488−6489. (f) Huang, M. H.; Dunn, B. S.; Soyez, H.; Zink, J. I. *Langmuir* **1998**, *14*, 7331−7333. (g) Minoofar, P. N.; Dunn, B. S.; Zink, J. I. *J. Am. Chem. Soc.* **2005**, *127*, 2656−2665. (h) Huang, M. H.; Dunn, B. S.; Zink, J. I. *J. Am. Chem. Soc.* **2000**, *122*, 3739−3745.
(28) (a) Lim, M. H.; Blanford, C. F.; Stein, A. *J. Am. Chem. Soc.* **1997**, *119*, 4090−4091. (b) Haller, I. *J. Am. Chem. Soc.* **1978**, *100*, 8050−8055.

Scheme 2. Procedures for the Construction and Operation of the Nanovalves **1a/b**-OUT[a]

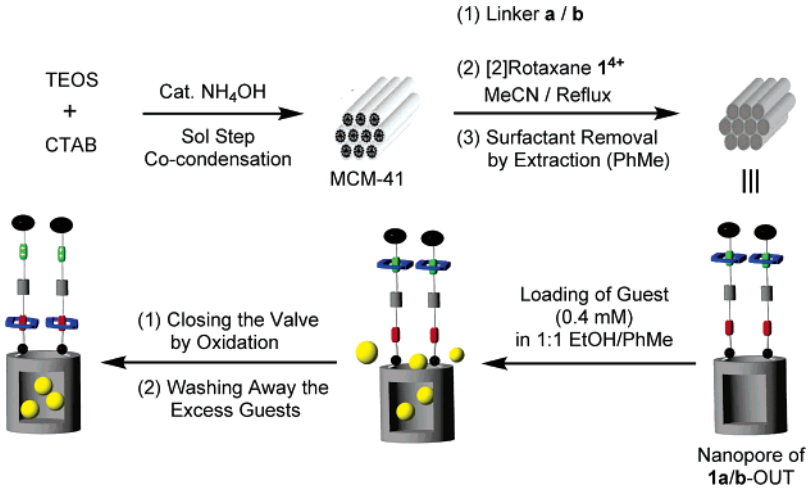

[a] First, TEOS and CTAB are co-condensed in the presence of a catalytic amount of NH_4OH to afford the silica particles MCM-41. Derivatization with the linker **a** or **b** and then the bistable [2]rotaxanes $\mathbf{1}^{4+}$, followed by an extraction with PhMe, affords the **1a**/**b**-OUT nanovalves. The nanovalves **1a**/**b**-OUT are loaded with guest molecules and closed by oxidation on the TTF site.

in H_2O (50 mL), followed by slow heating. After the solution had cooled down to room temperature, concentrated NH_3 solution (16 mL) and EtOH (75 mL) were added successively. The mixture was stirred rapidly for 15 min. TEOS (4.9 mL) and allyltriethoxysilane **b** (0.45 mL) were added rapidly while stirring. The solution was stirred for a further 2 h. The white precipitate was filtered and washed with H_2O (2 × 50 mL) and MeOH (2 × 50 mL). The material was dried under reduced pressure. Solvent extraction was carried out by refluxing the material (0.77 g) in MeOH/HCl solution (100 mL/0.5 mL concentrated HCl) for 20 h. The material was filtered and dried under reduced pressure. To obtain the N_2 isotherms, the material was dried further at 90 °C for 4 h.

Positioning the Linker with the IN_{CD} and IN_{SED} Locations. MCM-41 was prepared by Grun's method and surfactant was removed by either solvent extraction or calcination as described previously. The material was filtered and dried under reduced pressure. Derivatization with the silane linker **b** was carried out using a gas-phase reaction (the powder was placed on a filter above the solution, refluxing linker **b** (1 mL) in PhMe (60 mL) for 12 h under N_2 (1 atm)).[28b] The material was filtered and soaked in PhMe for 1 d to remove the excess of surface-adsorbed linkers. The resulting material was washed, filtered, and dried under reduced pressure.

Positioning the Linker with the OUT Location. MCM-41 prepared by Grun's method with the surfactant still inside the nanopores was derivatized with linkers using the gas-phase reaction described in Scheme 2. After washing with PhMe, the surfactant was removed by solvent extraction. The important difference between the syntheses of the IN_{SED} and the OUT locations is the reverse order of the linker derivatization and the solvent extraction steps.

Controlled Release Experiments. The release of probe molecules from the nanopores into the supernatant was measured by monitoring the emission spectrum of the probe molecules in the solution above the MCM-41 powder over time (release profile). A sample containing 30 mg of SiO_2 in MeCN (10 mL) was placed in a cell holder in such a way that only the MeCN solution was exposed to excitation light. The solution containing the released probe molecules was excited at 351 nm and its luminescence was monitored over time. The solution was stirred slowly. Ascorbic acid (reductant, in 1:1 EtOH/PhMe, 30 μL, 2 equiv for each rotaxane) was added at a designated time to open the nanovalves.

Acknowledgment. The research was conducted as part of an NSF-NIRT program and DMR 0346610. T.D.N. acknowledges the award of a UCLA Dissertation Year Fellowship and discussions with Yaroslav Klichko, Lars Erik Johansson, Sarah Angelos, Monty Liong, and Dr. Xianghuai Wang. We thank Professor Bruce Dunn and Grant Umeda for use of the Accelerated Surface Area and Porosimetry Analyzer for obtaining N_2 isotherms. We are grateful for the instruction given by Professor Yang Yang, Dr. Chih-Wei Chu, and Yan Yao in the operation of the reflectance FT-IR spectrometer. We thank Professor Mark Thompson for providing $Ir(ppy)_3$. The powder XRD instrument used in this work was obtained under equipment grant number DMR-0315828.

Supporting Information Available: Details of reflectance infrared spectra, nitrogen absorption/desorption isotherms, XRD patterns of the surfactant-removed MCM-41 porous silica particles, and fluorescence spectra of the bistable [2]rotaxane $\mathbf{1}^{4+}$ in MeCN and when tethered to MCM-41; complete ref 3d. This material is available free of charge via the Internet at http://pubs.acs.org.

JA065485R